



## Ionospheric depletion in auroral downward currents

Alexandra P. Cran-McGreehin,<sup>1</sup> Andrew N. Wright,<sup>1</sup> and Alan W. Hood<sup>1</sup>

Received 15 February 2007; revised 21 May 2007; accepted 13 July 2007; published 25 October 2007.

[1] The auroral downward field-aligned current is mainly carried by electrons of ionospheric origin accelerated into the magnetosphere along the Earth's high-latitude field lines. The ionosphere is a finite source of electrons: Thus, if a current is to continue to flow, it is natural to assume that the current region must broaden to access more current carriers. In this paper, we present an Alfvén wave model of magnetosphere-ionosphere interaction to describe the evolution of ionospheric E region number density under the influence of a downward current. The behavior of the system falls into two regimes depending upon whether the quantity  $\mathcal{W} = j_{\parallel 0} / \alpha n_e^2 h$  is greater or less than unity (where  $j_{\parallel 0}$  is initial current density,  $\alpha$  is the recombination coefficient,  $n_e$  is background E region number density, and  $h$  is E region height): If the current density is smaller than a critical current density,  $j_c = \alpha n_e^2 h$  (i.e.,  $\mathcal{W} < 1$ ), then the E region only depletes within the original current region, and there is sufficient photoionization to feed the current to the magnetosphere; if the required current density is larger than  $j_c$  (i.e.,  $\mathcal{W} > 1$ ), then the current region is forced to broaden in order to access sufficient electrons. On the dayside, where a typical E region number density is  $\sim 10^{11} \text{ m}^{-3}$ , broadening only occurs for very strong current densities  $\sim 10 \mu\text{A m}^{-2}$ ; on the nightside, however, where E region number densities can fall by a factor of 10, broadening occurs for any current density greater than  $\sim 0.1 \mu\text{A m}^{-2}$ . From this model, we derive expressions for the final depletion width (generally  $\sim 1$ – $10$  times the width of the original current region) and for the characteristic timescale of depletion (typically  $\sim 10$ – $100$  s).

**Citation:** Cran-McGreehin, A. P., A. N. Wright, and A. W. Hood (2007), Ionospheric depletion in auroral downward currents, *J. Geophys. Res.*, 112, A10309, doi:10.1029/2007JA012350.

### 1. Introduction

[2] Earth's field-aligned currents (FACs) couple the magnetosphere and ionosphere, and interest in them was originally sparked by the remarkable northern lights. The visible aurora is caused by the upward FAC, where electrons of magnetospheric origin are accelerated downward along high-latitude field lines, supported by large inverted-V converging electric field structures. There have been many observations and studies of these upward FACs, but the nature of their downward counterparts was not well understood until the advent of the FAST satellite in 1996 and the Cluster mission in 2001. These spacecraft, with their higher spatial and temporal resolution, have been able to identify many examples of the narrower-scale, temporal downward FACs, which often exist at the edge of the larger upward current regions.

[3] Many models of both the upward [e.g., Knight, 1973; Wright and Hood, 2003; Vedin and Rönmark, 2004] and downward [e.g., Jasperse, 1998; Temerin and Carlson, 1998; Cran-McGreehin and Wright, 2005a, 2005b] FAC regions assume a steady state. This is justified in the upward current region, since the source of electrons in this case is

the magnetosphere which can give an almost limitless supply; indeed, Wright *et al.* [2002] estimate that less than 5% of magnetospheric electrons would be removed from a flux tube during the upward current phase of a  $\mu\text{A m}^{-2}$  ULF field line resonance (approximately minutes). The situation in downward current regions is very different. As electrons are accelerated upward from the ionosphere, ions also travel away horizontally through the E region to carry the Pedersen current: Thus the E region electron and ion number densities quickly erode during a downward current. Such suppressed densities have been observed by EISCAT radar data in downward current regions by Aikio *et al.* [2002, 2004]. In a simple calculation, a steady downward current density of  $1 \mu\text{A m}^{-2}$  leads to an outflow of electrons of  $6.2 \times 10^{12} \text{ m}^{-2} \text{ s}^{-1}$ . The nightside E region typically has a number density of  $10^{10} \text{ m}^{-3}$  and a height of 20 km, resulting in a height-integrated number density of  $2 \times 10^{14} \text{ m}^{-2}$ . Thus the upward electron flow will result in total E region density erosion in  $\sim 30$  s. Although this calculation does not take production processes, such as photoionization, into account, it illustrates that a modest downward current may significantly deplete the electron supply at the ionospheric foot point, and raises the possibility that the current region may need to broaden in order to access more current carriers. Aikio *et al.* [2004] observed exactly this phenomenon with Cluster: The downward current region widened over a

<sup>1</sup>Mathematical Institute, University of St. Andrews, Fife, UK.

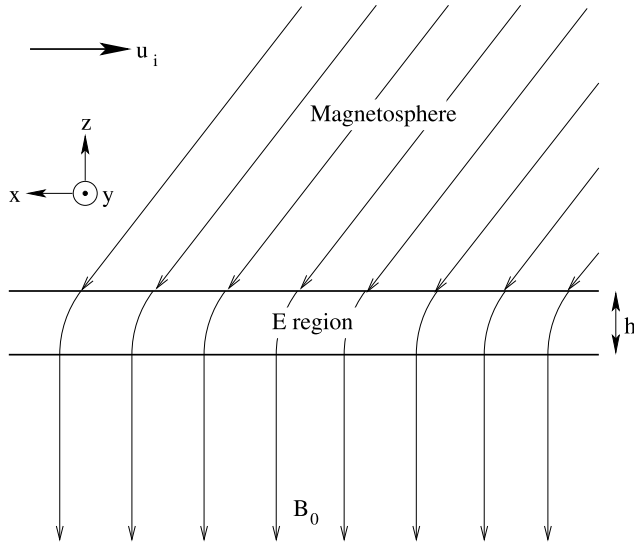


**Figure 1.** Diagram of the  $x$ - $z$  plane of the model, adapted from *Wright* [1996]. Incoming Alfvén waves in the magnetosphere have velocity  $-u_i \hat{x}$  and magnetic field perturbation  $b_i \hat{x}$ . These waves are partially reflected at the magnetosphere-E region interface.

period of  $\sim 70$  s in order to continue to carry the required current.

[4] A similar situation has also been observed by *Marklund et al.* [2001] using the four Cluster spacecraft; their Figure 3 shows the event which took place at 0336 MLT on 14 January 2001 at  $\sim 21,000$  km altitude and at a magnetic latitude of  $69.8^\circ$ . When the first spacecraft flew through, it detected a compact downward current region with a peak current density of  $\sim 0.16 \mu\text{A m}^{-2}$  (*Marklund et al.*'s Figure 3 (middle), Rumba). As subsequent spacecraft flew through the same region over a period of 280 s, a broadening of the downward current region was seen, with lower current densities but roughly the same overall current being carried. The associated bipolar perpendicular electric field signature, indicative of an accelerating potential beneath the spacecraft, initially grew to  $\sim 25 \text{ mV m}^{-1}$  and then disappeared altogether by the final crossing. These data support the idea that evacuation of the E region during a downward current forces the current region to broaden in time in order to continue to carry the same total current. *Karlsson and Marklund* [1998] have modeled this phenomenon by imposing current closure on a small-scale ( $\sim 10$  km) field-aligned current pair, and found that current densities of the order of  $10 \mu\text{A m}^{-2}$  created deep density cavities in the E and lower F regions on timescales of the order of seconds. *Blixt and Brekke* [1996] also used the idea of current closure to model a discrete auroral arc, neglecting the effects of photoionization and recombination in the ionosphere, and also found ionospheric density depletion in the downward current region. *Doe et al.* [1995] presented a two-dimensional (2-D) model of the ionosphere under the effects of various gain and loss mechanisms, including a field-aligned current pair imposed at the top of the ionosphere. They found that modest downward current densities of 0.2 and  $0.02 \mu\text{A m}^{-2}$

could create cavities on timescales from 30 to 64 s, respectively.

[5] The dynamics of propagating Alfvén waves coupling the magnetosphere and ionosphere have been extensively studied in the upward current region, where electron precipitation leads to conductivity enhancements and gradients in the ionosphere. These drive a nonlinear feedback process that produces small-scale auroral arcs [*Pokhotelov et al.*, 2002; *Lysak and Song*, 2002; and *Streltsov and Lotko*, 2005]. *Streltsov and Marklund* [2006] have applied the theory of Alfvén waves to the downward current region in a numerical simulation, which reveals characteristic features such as a decrease with time in the amplitude of the parallel electric field, and broadening of the current region. In this paper, we model the evacuation of electrons from the E region for a downward current using the ideas of Alfvén wave propagation and reflection at the magnetosphere-ionosphere boundary, which lead to decreased conductivities and a necessary broadening of the current region, which we see is achieved through a change in reflection coefficient. Although our modeling of the ionosphere is simpler than that of *Doe et al.* [1995], the added advantage of our model is that it includes feedback from the ionosphere to the magnetosphere through the Alfvén wave reflection coefficient.

## 2. Introducing the Model

### 2.1. Physical Description

[6] We use a 2-D Cartesian system (invariant in  $x$ ) to model the E region electron evacuation in the downward current region. Figure 1 shows a slice of the model in the  $x$ - $z$  plane: Incoming Alfvén waves with velocity in the  $x$  direction partially reflect at the magnetosphere-E region interface. The E region, of height  $h$ , is initially undepleted. The E region number density is subject to gain due to photoionization and loss due to recombination. At equilibrium, when no current is drawn, these two effects balance one another.

[7] Figure 2 shows the  $y$ - $z$  plane of the model: A shear in the incident Alfvén speed ( $u_i$ ) in the  $y$  direction leads to the formation of a downward field-aligned current ( $j_{\parallel}$ ), such that electrons are drawn up from the E region with velocity  $v_{e\parallel} \hat{z}$  and ions travel away horizontally with velocity  $\pm v_{i\perp} \hat{y}$  to carry the Pedersen current. Thus the downward field-aligned current acts as another loss mechanism to the E region number density, causing the formation of a depleted region. The resulting decrease in conductivity in this depleted region modifies the reflection coefficient and hence affects the reflected Alfvén waves. The evolution of the system is modeled via a number density continuity equation in the E region, which incorporates changes to the number density due to photoionization, recombination and downward field-aligned current caused by the shear flow in the magnetosphere.

### 2.2. Governing Equations

[8] As used by *Streltsov and Lotko* [2005] to study upward currents, the plasma continuity equation in the E region of the ionosphere is given by

$$\frac{\partial n}{\partial t} = \frac{j_z}{eh} + \alpha(n_e^2 - n^2) \quad (1)$$

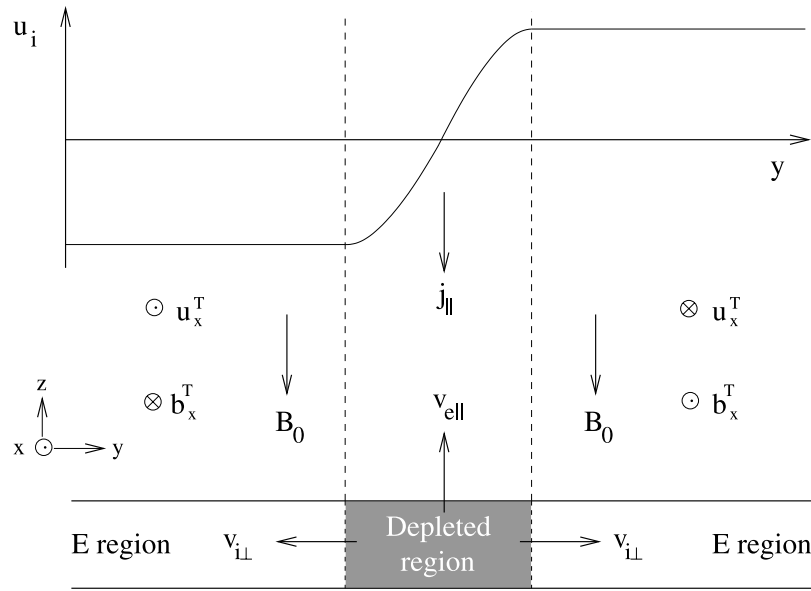


**Figure 2.** Diagram of the  $y$ - $z$  plane of the model. A shear in the incident Alfvén velocity ( $-u_i \hat{x}$ ) in the  $y$  direction generates a downward field-aligned current. This draws electrons upward from the E region, while ions travel away horizontally to carry the Pedersen current, leaving a region of depleted number density. The total Alfvén wave velocity perturbation ( $u_x^T$ ) and magnetic field perturbation ( $b_x^T$ ) change sign across the incident velocity shear.

where  $n$  is electron number density,  $n_e$  is equilibrium electron number density,  $j_z$  is field-aligned current density,  $h$  is the height of the E region, and  $\alpha$  is the recombination coefficient which we take to be  $\sim 3 \times 10^{-13} \text{ m}^3 \text{ s}^{-1}$  [Ulich *et al.*, 2000]. While stratified models for  $\alpha$  exist [Vickrey *et al.*, 1982], we use an average value to retain analytical results.

[9] In this equation,  $\alpha n_e^2$  is a source term corresponding to UV photoionization. Thus this term implies that more photoionization occurs during the day (when  $n_e \sim 10^{11} \text{ m}^{-3}$ ) than at night (when  $n_e \sim 10^{10} \text{ m}^{-3}$ ); this is logical, as photoionization will be inhibited at night when the ionosphere is not directly sunlit. This term also indicates that the photoionization rate is constant for a given  $n_e$ ; this can be justified, since the rate depends on the incident radiation and E region neutral number density, both of which can be taken to be constant on the timescales involved in this model ( $\sim$ minutes). The loss term,  $-\alpha n^2$ , represents dissociative recombination of ions, predominantly  $\text{NO}^+$  and  $\text{O}_2^+$ , in the E region.

[10] Equation (1) can be integrated in the  $z$  direction over the height of the ionosphere, assuming that there is no variation in the  $x$  direction and that  $n$  is also independent of  $z$ , yielding

$$\frac{\partial N}{\partial t} - \frac{j_z(y, z = h, t)}{e} = \frac{\alpha}{h} (N_e^2 - N^2) \quad (2)$$

where  $N(y, t) = \int n(y, z) dz$  is the height-integrated number density of the E region, and  $N_e = \int n_e dz$  is the equilibrium value.

[11] In models of the ionospheric feedback instability [e.g., Lysak and Song, 2002], where electrons are precipitating into the ionosphere to carry an upward current, the

$j_z$  term serves as a source of electrons in the E region; in our model of the downward current region, it is a loss term. We drive the field-aligned current  $j_z$  in equation (2) by a shear flow in the magnetosphere, as shown in Figure 2. The incident Alfvén wave is reflected from the ionosphere, and the incident and reflected waves add to give a total perpendicular magnetic field component ( $b_x^T \hat{x}$ ) and velocity ( $u_x^T \hat{x}$ ). The shear in incident Alfvén velocity perturbation ( $-u_i(y) \hat{x}$ ) shown in Figure 2 gives rise to a shear in  $b_x^T$ , consistent with the parallel current density via Ampère's law. The boundary condition between the ideal magnetosphere and the nonideal, stationary ionosphere is given by [e.g., Wright, 1996]

$$b_x^T = \mu_0 \Sigma_p u_x^T B_0 \quad (3)$$

where  $\mu_0$  is the permittivity of a vacuum,  $\Sigma_p$  is the height-integrated Pedersen conductivity, and  $B_0$  is the background magnetic field strength. For incident magnetic field and velocity perturbations,  $b_i \hat{x}$  and  $-u_i \hat{x}$ , this yields a reflection coefficient [Malinckrodt and Carlson, 1978],

$$r = \frac{1 - \mu_0 \Sigma_p V_A}{1 + \mu_0 \Sigma_p V_A} \quad (4)$$

where  $V_A = B_0 / \sqrt{\mu_0 \rho_0}$  is the Alfvén speed, and  $\rho_0 = n_0 m_i$  is the uniform magnetospheric ion mass density,  $n_0$  being magnetospheric ion number density and  $m_i$  being ion mass. This gives expressions for the total wave magnetic field and velocity perturbations:

$$b_x^T = \frac{2b_i \mu_0 \Sigma_p V_A}{1 + \mu_0 \Sigma_p V_A} \quad (5)$$

$$u_x^T = \frac{2u_i}{1 + \mu_0 \Sigma_p V_A} \quad (6)$$

We assume a linear relationship between  $\Sigma_p$  and  $N$ , such that  $\Sigma_p = \Sigma_{P0} N / N_e$ , where  $\Sigma_{P0}$  represents the equilibrium height-integrated Pedersen conductivity when  $N = N_e$ . Using this expression, that for  $V_A$ , and the fact that  $b_i = u_i \sqrt{\mu_0 \rho_0}$  for an Alfvén wave propagating parallel to the background magnetic field (i.e., northern hemisphere), we can rewrite equation (5) as

$$b_x^T = \frac{2\mu_0 B_0 u_i \Sigma_{P0} N}{N_e \left( 1 + \sqrt{\frac{\mu_0}{\rho_0}} \Sigma_{P0} B_0 \frac{N}{N_e} \right)} \quad (7)$$

Differentiating expression (7) with respect to  $y$  and using Ampère's law, we see that

$$\frac{j_z}{e} = -N_e \frac{\partial}{\partial y} \left( \frac{\eta u_i \bar{N}}{1 + \beta \bar{N}} \right) \quad (8)$$

where

$$\eta = \frac{2\Sigma_{P0} B_0}{N_e e}, \quad (9)$$

$$\beta = \sqrt{\frac{\mu_0}{\rho_0}} \Sigma_{P0} B_0 \quad (10)$$

and

$$\bar{N} = \frac{N}{N_e} \quad (11)$$

Substituting equation (8) into (2), we have a partial differential equation such that

$$\frac{\partial \bar{N}}{\partial \bar{t}} + \frac{\partial}{\partial \bar{y}} \left( \frac{\eta \bar{u}_i \bar{N}}{1 + \beta \bar{N}} \right) = \bar{\alpha} (1 - \bar{N}^2) \quad (12)$$

Equation (12) has been normalized by using

$$\bar{y} = \frac{y}{y_0} \quad (13)$$

$$\bar{u}_i = \frac{u_i}{u_{i0}} \quad (14)$$

and

$$\bar{t} = \frac{t}{\tau} = \frac{u_{i0} t}{y_0} \quad (15)$$

where  $y_0$  is the characteristic length scale,  $u_{i0}$  is the amplitude of the incoming Alfvén wave, and  $\tau = y_0 / u_{i0}$  is a

characteristic timescale. The recombination coefficient,  $\alpha$ , has been normalized to give

$$\bar{\alpha} = \frac{\alpha y_0 N_e}{u_{i0} h} \quad (16)$$

[12] Taking typical ionospheric parameters of  $\Sigma_{P0} = 1$  mho,  $B_0 = 5 \times 10^4$  nT,  $n_e = 5 \times 10^{10} \text{ m}^{-3}$  and  $h = 20$  km yields  $N_e = 10^{15} \text{ m}^{-2}$ , and  $n_0 = 10^6 \text{ m}^{-3}$  gives  $\rho_0 = 1.67 \times 10^{-21} \text{ kg m}^{-3}$  in the magnetosphere. These values lie within the range of parameters used in many ionosphere-magnetosphere interaction models at high latitudes [e.g., *Sato*, 1978; *Miura and Sato*, 1980], and give  $\beta = 1370$  and  $\eta = 3.12$ , which we will use in the rest of this paper, unless stated otherwise.

### 3. Numerical Solution

[13] We first solve the partial differential equation in (12) numerically. We take an initially undepleted ionosphere with  $N = N_e$  everywhere, and  $\bar{u}_i = \tanh \bar{y}$  giving an initial current density magnitude,  $j_{\parallel}$ , which can be determined from equation (8) to be

$$j_{\parallel} = \frac{N_e e u_{i0}}{y_0} \left( \frac{\eta}{1 + \beta} \right) \text{sech}^2 \bar{y} \quad (17)$$

The maximum initial current density,  $j_{\parallel 0}$ , occurs at  $\bar{y} = 0$  and is given by

$$j_{\parallel 0} = \frac{N_e e u_{i0}}{y_0} \frac{\eta}{1 + \beta} \approx \frac{2u_{i0}}{y_0} \sqrt{\frac{\rho_0}{\mu_0}} \quad (18)$$

when  $\beta \gg 1$ , while the maximum magnetic field perturbation occurs as  $y \rightarrow \infty$  and is given by

$$b_{x0}^T = \mu_0 N_e e u_{i0} \frac{\eta}{1 + \beta} \quad (19)$$

In all of the following work, the symmetry about the  $y$  axis is exploited, and only the region  $y > 0$  is shown. We use a first-order backward differencing method to solve this system, since it is suitable for evolving any shocks that develop. The accuracy of the code was tested for two resolutions, and the relative error was never greater than  $\sim 0.5\%$ . In the results presented here,  $\delta \bar{y} = 0.01$  and  $\delta \bar{t} = 0.001$ .

[14] Using the parameter values listed above, Figure 3 shows the evolution of the number density in time for four different initial current densities. All of these cases reach a steady state when the ionization rate matches the combined loss rate due to recombination and downward current being drawn. The smallest current density of  $2 \mu\text{A m}^{-2}$  in Figure 3a only requires a partial depletion of the initial shear width  $\sim y_0$  before a steady state is reached. In Figure 3b, where  $j_{\parallel 0} = 3 \mu\text{A m}^{-2}$ , we can see that the number density depletes down to approximately zero at  $\bar{y} = 0$ , when the system then develops a shock as it requires a slight broadening of the depletion region in order to carry the current. The larger current densities of 8 and  $15 \mu\text{A m}^{-2}$  in Figures 3c and 3d require even more broadening and exhibit a shock feature which moves out as the system requires to access more current carriers from adjacent regions.

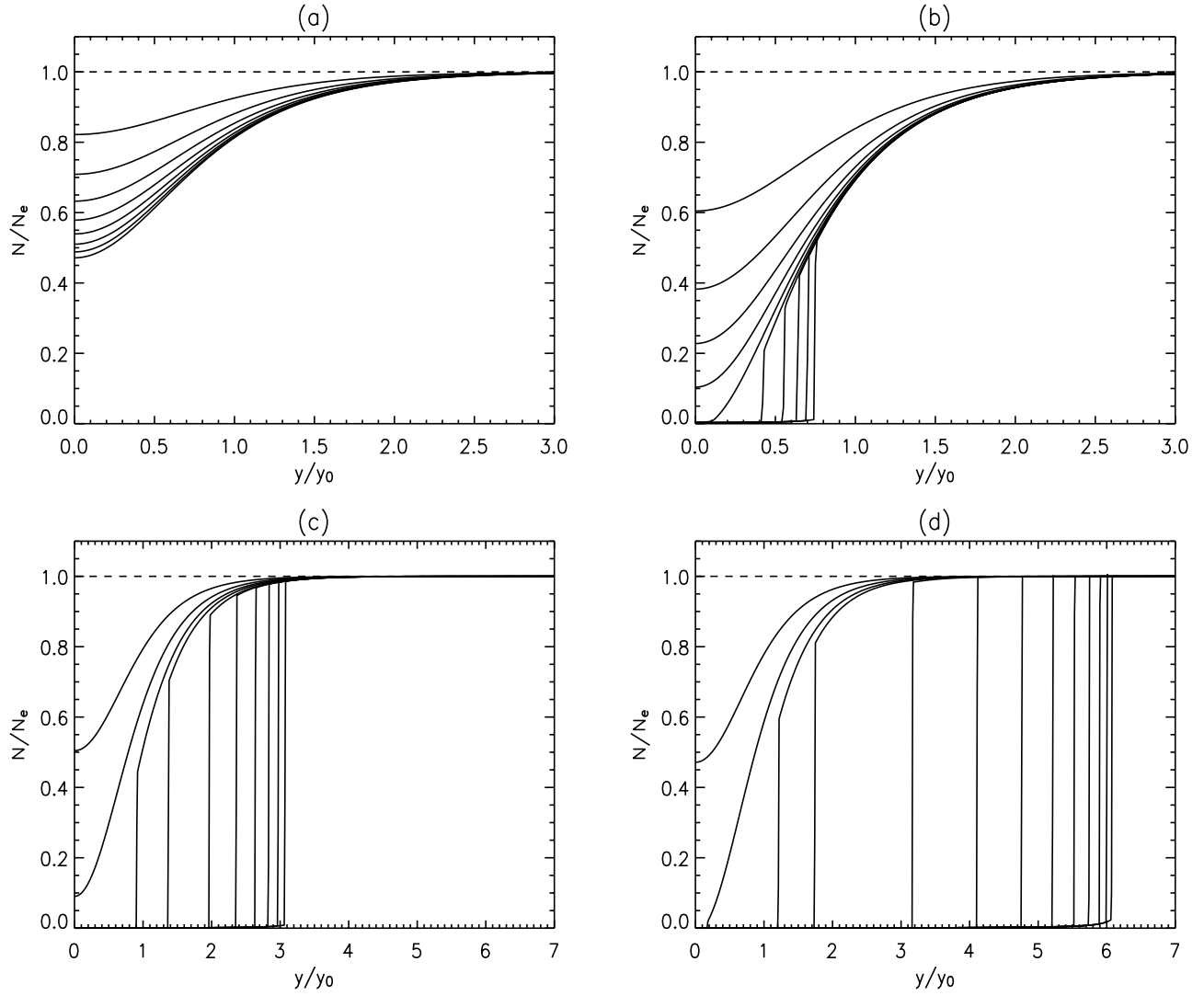


**Figure 3.** Number density evolution in time for  $j_{\parallel 0}$  ( $\mathcal{W}$ , defined later in equation (32)) values of (a)  $2.0 \mu\text{A m}^{-2}$  (0.832); (b)  $3.0 \mu\text{A m}^{-2}$  (1.25); (c)  $8.0 \mu\text{A m}^{-2}$  (3.33); and (d)  $15.0 \mu\text{A m}^{-2}$  (6.24). The number density profiles shown are for  $t = 18.2, 36.5, 54.7, 72.9, 91.2, 109.4, 127.6,$  and  $145.8$  s (Figure 3a);  $30.4, 60.8, 91.2, 121.5, 151.9, 182.3, 212.7, 243.1, 273.5,$  and  $303.8$  s (Figure 3b);  $11.4, 22.8, 34.2, 45.6, 68.4, 91.2, 113.9, 136.7, 159.5,$  and  $182.3$  s (Figure 3c); and  $6.1, 12.2, 18.2, 24.3, 48.6, 72.9, 97.2, 121.5, 145.8, 170.2, 194.5, 218.8,$  and  $243.1$  s (Figure 3d). Smaller current densities only cause a partial depletion of the E region, whereas for larger current densities the region of depletion must spread out in order to access sufficient current carriers.

[15] The evolution of the magnetic field perturbations is shown in Figure 4 (top) for two different initial current densities of 3 and  $8 \mu\text{A m}^{-2}$ . The discontinuity in  $\bar{N}$  which moves out from the origin with time is associated with a discontinuity in  $b_x^T$ : As a result of this, there is a surface current at the shock. However, what happens once the steady state is reached? The partial differential equation in (12) reduces to

$$\frac{\partial}{\partial \bar{y}} \left( \frac{\eta \bar{u}_i \bar{N}}{1 + \beta \bar{N}} \right) = \frac{1}{N_e e \mu_0 u_{i0}} \frac{\partial b_x^T}{\partial \bar{y}} = \bar{\alpha} (1 - \bar{N}^2) \quad (20)$$

This tells us that  $b_x^T(y, t \rightarrow \infty)$  is continuous, so there is no surface current in the final steady state. The depleted region

has a width denoted by  $\bar{W}_s$ . Within this depleted region,  $\bar{N} \ll 1$ , and thus we have that

$$\frac{1}{N_e e \mu_0 u_{i0}} \frac{\partial b_x^T}{\partial \bar{y}} = \bar{\alpha} \quad (21)$$

$$\Rightarrow b_x^T = \bar{\alpha} N_e e \mu_0 u_{i0} \bar{y} \quad (22)$$

Outside the depleted region, where  $\bar{y} > \bar{W}_s$ , we have that  $\beta \bar{N} \gg 1$ , and equation (20) reduces to

$$\frac{\partial}{\partial \bar{y}} \left( \frac{\eta \bar{u}_i}{\beta} \right) = \frac{1}{N_e e \mu_0 u_{i0}} \frac{\partial b_x^T}{\partial \bar{y}} \quad (23)$$

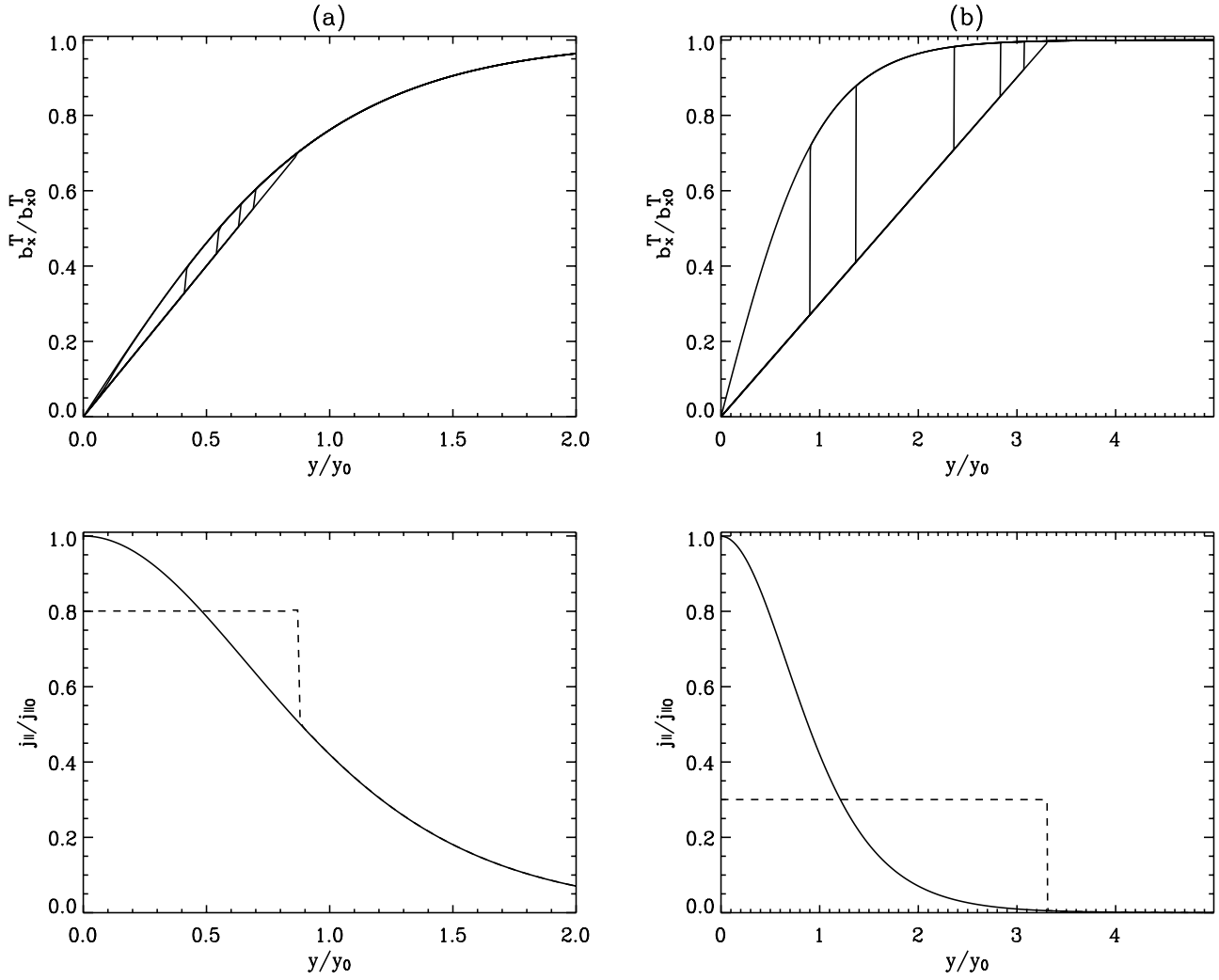


**Figure 4.** Evolution of (top) magnetic field perturbation and (bottom) current density in time for  $j_{||0}$  values of (a)  $3.0 \mu\text{A m}^{-2}$  and (b)  $8.0 \mu\text{A m}^{-2}$ . Magnetic field perturbation profiles shown are for  $t = 0, 151.9, 182.3, 212.7, 243.1, 273.5,$  and  $546.9$  s (Figure 4a); and  $0, 34.2, 45.6, 91.2, 136.7, 182.3,$  and  $364.6$  s (Figure 4b). Initial (solid line) and steady state (dashed line) current densities are shown for both cases.

$$\Rightarrow b_x^T = N_e e \mu_0 u_{i0} \frac{\eta}{\beta} \tanh \bar{y} \quad (24)$$

[16] In the steady state, these two expressions for  $b_x^T$  must match at  $\bar{W}_s$ , telling us that

$$\mathcal{W} \tanh \bar{W}_s = \bar{W}_s \quad (25)$$

where

$$\mathcal{W} = \frac{\eta}{\bar{\alpha} \beta} \quad (26)$$

This gives an implicit equation for the steady state position of the number density shock. Figure 4 (bottom) shows the initial (solid line) and final (dashed line) current densities

for the two cases. The area under initial and final curves is the same, since the total current in a given case remains constant. Given that  $b_x^T$  is linear in the depleted region, the current density is constant there. In the first case, where  $j_{||0} = 3 \mu\text{A m}^{-2}$ , not much spreading of the current density occurs; the effect is much more obvious in the second case, where  $j_{||0} = 8 \mu\text{A m}^{-2}$ . We also see that the maximum magnitude of the parallel current density decreases in time, a feature also observed in the Cluster data of *Marklund et al.* [2001].

## 4. Analytical Results

### 4.1. Depletion Width

[17] In this section, we wish to obtain analytical approximations for the width to which the depleted region spreads, and in the case where broadening occurs, the position of the shock in time. Our numerical simulations show that there are two regimes. For large initial current densities, the

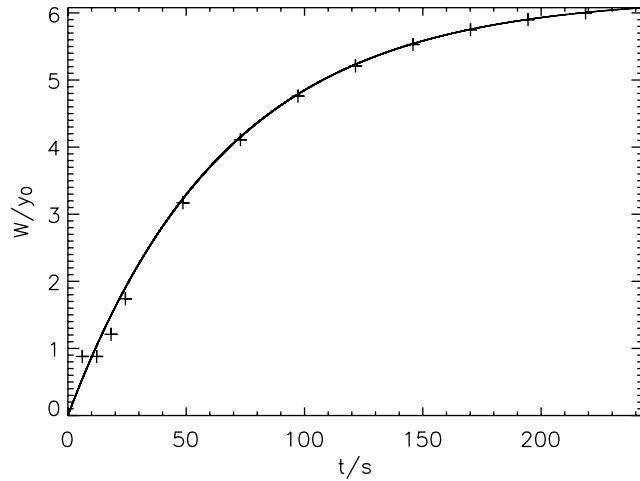


**Figure 5.** Plot of discontinuity position with time for  $j_{\parallel 0} = 15 \mu\text{A m}^{-2}$  obtained from the numerical simulation (crosses) and from the analytical expression in equation (31). The analytical expression is seen to be accurate once the depleted region extends beyond the original shear width,  $y_0$  at  $t \sim 30$  s.

region of depleted density broadens to a depletion width that is larger than the original shear width (as in Figures 3c and 3d). For smaller initial current densities, only partial depletion occurs, and the depletion width is approximately equal to the initial velocity shear width (as illustrated by Figure 3a). We begin by considering the first of these two cases. As can be seen from Figures 3c and 3d, when significant depletion takes place, the recombination term can safely be ignored within the depleted region, since  $\bar{N} \approx 0$  there. Thus, integrating equation (12), we obtain

$$\int_{y=0}^{\infty} \frac{\partial \bar{N}}{\partial t} + \frac{\partial}{\partial y} \left( \frac{\eta \bar{u}_i \bar{N}}{1 + \beta \bar{N}} \right) dy = \bar{\alpha} \int_{y=0}^{\infty} 1 - \bar{N}^2 dy \quad (27)$$

Noting that  $\beta \gg 1$ ,  $\bar{u}_i(0) = 0$  and  $\lim_{y \rightarrow \infty} \bar{u}_i = 1$ , and assuming that the discontinuity jumps from a curve  $\bar{N}_-$  to another curve  $\bar{N}_+$ , we obtain

$$\begin{aligned} \frac{\partial}{\partial t} \left( \int_0^{\bar{W}(t)} \bar{N}_- dy + \int_{\bar{W}(t)}^{\infty} \bar{N}_+ dy \right) + \frac{\eta}{\beta} \\ = \bar{\alpha} \left( \int_0^{\bar{W}(t)} 1 - \bar{N}_-^2 dy + \int_{\bar{W}(t)}^{\infty} 1 - \bar{N}_+^2 dy \right) \end{aligned} \quad (28)$$

where  $\bar{W}$  is the position of the shock in time. If we now assume that  $\bar{N}_- \approx 0$  and that  $\bar{N}_+ \approx 1$ , which is valid once the discontinuity has moved beyond  $\sim y_0$  (the original shear width), then this reduces to

$$\frac{\partial \bar{W}}{\partial t} = \frac{\eta}{\beta} - \bar{\alpha} \bar{W} \quad (29)$$

We can solve this by noting that if the final depletion width  $\bar{W}_s > 1$ , then  $\tanh \bar{W}_s \approx 1$ , and equation (25) tells us that

$$\lim_{t \rightarrow \infty} \bar{W} = \bar{W}_s = \mathcal{W} \quad (30)$$

We can then obtain an expression for the evolution of the width of the depleted region in time:

$$\bar{W}(t) = \mathcal{W}(1 - e^{-\bar{\alpha}t}) \quad (31)$$

Figure 5 compares the expression for  $\bar{W}$  in equation (31) with simulation values for a current density of  $15 \mu\text{A m}^{-2}$ , the same case as that shown in Figure 3d. It shows that the expression is a very good approximation once the discontinuity has moved beyond the original shear width,  $y_0$ .

[18] Substituting equations (16) and (18) into the expression for  $\mathcal{W}$  in equation (26), we can see that

$$\mathcal{W} = \frac{h j_{\parallel 0}}{\alpha e N_e^2} = \frac{j_{\parallel 0}}{\alpha e n_e^2 h} \quad (32)$$

Thus the width can be seen to increase linearly with current density: A larger current density requires more current carriers and thus a wider depletion width. The width is inversely proportional to  $\alpha$  and  $h$ ; a smaller photoionization rate produces fewer electrons per unit area, and so the depletion region will broaden more before a steady state is reached; and a decreased ionospheric height also provides fewer electrons, resulting in a higher depletion width. The depletion width also increases as the ionospheric number density decreases, since this implies fewer current carriers per unit volume; indeed,  $\mathcal{W}$  is more sensitive to changes in  $n_e$  than to changes in any of the other parameters.

[19] The depletion width in equation (32) can be used to determine whether broadening occurs for a given system: Significant broadening occurs when  $\mathcal{W} > 1$ , and no broadening occurs when  $\mathcal{W} < 1$ . Thus it is the value of  $\mathcal{W}$  for a given system which determines the nature of the solution. In

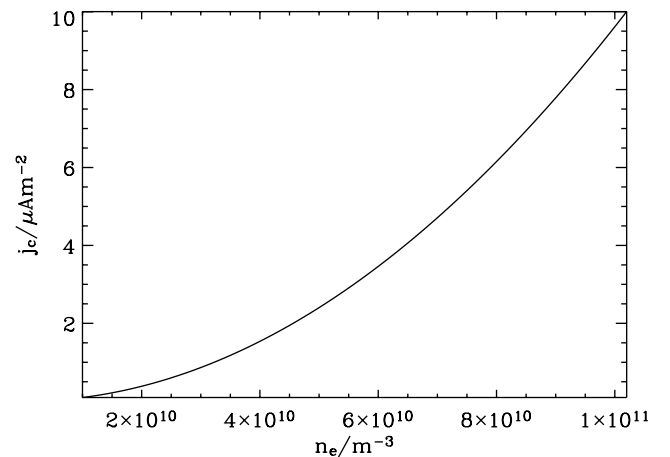


**Figure 6.** Variation of  $j_c$  with E region number density for typical parameters  $h = 2 \times 10^4$  m and  $\alpha = 3 \times 10^{-13} \text{ m}^3 \text{ s}^{-1}$ . This shows that significant E region depletion should be far more common on the nightside (with lower ionospheric number densities) than on the dayside.

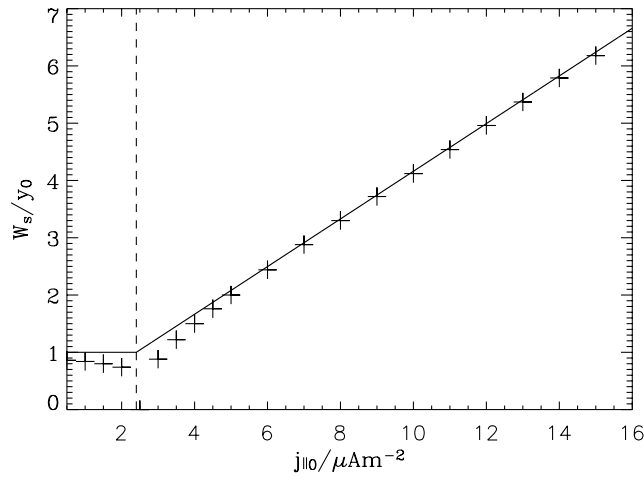


**Figure 7.** Simulation steady state depletion widths (crosses) and estimate (solid line) from equation (34) for varying initial current densities, using  $n_e = 5 \times 10^{10} \text{ m}^{-3}$  and  $h = 20 \text{ km}$ . The estimate is seen to be very reliable.

Figure 3, we fixed the ionospheric parameters ( $\alpha$ ,  $n_e$  and  $h$ ) and varied  $j_{\parallel 0}$  to obtain the different number density contours: However, we could have chosen any combination of parameters which gave  $\mathcal{W}$  values of 0.832, 1.25, 3.33 and 6.24 to generate the same curves. The timescales involved would, however, change. We can estimate the critical lowest current density,  $j_c$ , for which broadening begins to occur by substituting  $\mathcal{W} = 1$  into equation (32) to obtain

$$j_c = \frac{N_e^2 e \alpha}{h} = n_e^2 h e \alpha \quad (33)$$

As the number density of the E region increases, so does the minimum current density necessary to require a broadening of the depletion region, since more current carriers are available. The variation of  $j_c$  with  $n_e$  is illustrated in Figure 6. For our E region number density of  $5 \times 10^{10} \text{ m}^{-3}$ ,  $j_c \sim 2.5 \text{ } \mu\text{A m}^{-2}$ , so significant depletion will occur for even relatively small downward current densities. On the dayside, typical E region number densities can be higher  $\sim 10^{11} \text{ m}^{-3}$ : In this regime, significant depletion only begins to occur for downward currents of  $\sim 10 \text{ } \mu\text{A m}^{-2}$ , so only very strong events will cause significant density holes in the dayside E region. (We note that for strong current densities such as this, the ionosphere becomes susceptible to instabilities which heat the plasma and change  $\alpha$  [St.-Maurice and Laneville, 1998].) Nightside number densities can be a factor of 10 lower, and in this regime, broadening would occur even for current densities as low as  $0.1 \text{ } \mu\text{A m}^{-2}$ . Density cavities should therefore be far rarer on the dayside than on the nightside.

[20] When equation (32) yields a width less than  $y_0$ , we are in the regime where no significant broadening occurs beyond  $y_0$ , and we can instead give the estimate  $y_0$ , since this is the initial shear width. Thus our estimate for the depletion width,  $W_s$ , can be written as

$$W_s = \begin{cases} y_0 j_{\parallel 0} / j_c & : j_{\parallel 0} > j_c \\ y_0 & : j_{\parallel 0} \leq j_c \end{cases} \quad (34)$$

This estimate is plotted in Figure 7 for  $n_e = 5 \times 10^{10} \text{ m}^{-3}$ , along with depletion widths taken from numerical simulations for comparison. The width was estimated from simulations by the following method: If the minimum number density at steady state at the origin is  $N_{\min}$ , then the depletion width is defined to be the distance from the origin to the steady state number density curve at  $N = (N_e + N_{\min})/2$ . Figure 7 shows that the estimate in equation (34) is very accurate for depletion widths greater than the shear width ( $y_0$ ), and is good at predicting the current density for which broadening begins to be important. Figure 8 shows the variation of the depletion width estimate in equation (34) with E region number density for various initial current densities: As  $n_e$  increases, the depletion width required for a given current density decreases, as more current carriers are available. Depletion widths of  $\sim 10 y_0$  are required for lower E region number densities to carry these currents.

## 4.2. Depletion Time

[21] We also wish to understand the typical timescales involved in this system. It tends toward a steady state as  $t \rightarrow \infty$ , and to quantify this approach to a steady state, we calculate the number of electrons,  $A(t)$ , that have been depleted per meter at a time  $t$  via the following:

$$A(t) = \int_0^{\infty} N_e - N(y, t) dy \quad (35)$$

This corresponds to the area above the curves and below  $\bar{N} = 1$  in Figure 3.  $A(t)$  will asymptote to a limiting value,  $A_s$ , as the steady state is reached. Thus the characteristic depletion time,  $t_d$ , based on the simulations is taken to be the time at which  $A(t) = A_s/2$ .

[22] Analytically, insight into the timescales involved in this system can be gained by examining the partial differential equation (PDE) in equation (12) more thoroughly. On  $\bar{y} = 0$ , and assuming that  $\beta \gg 1$  and that  $\beta \bar{N} \gg 1$  (true for our parameters until  $\bar{N}$  falls to  $\sim 10^{-3}$ ), this PDE reduces to

$$\frac{\partial \bar{N}}{\partial t} = \bar{\alpha} (1 - \mathcal{W} - \bar{N}^2) \quad (36)$$

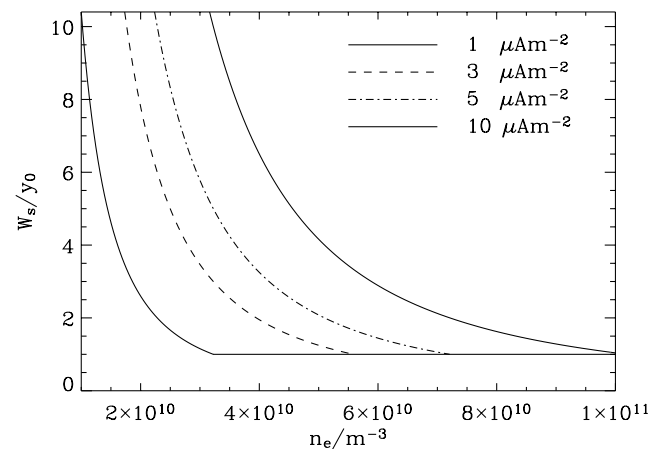


**Figure 8.** Variation of depletion width in equation (34) with E region number density for different initial current densities ( $j_{\parallel 0}$ ) and  $h = 20 \text{ km}$ .

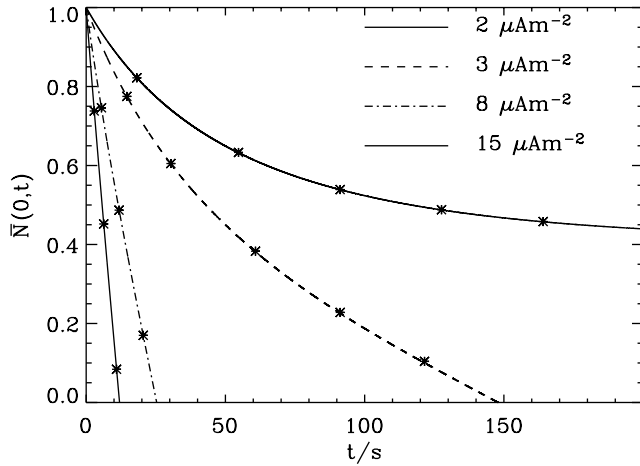


**Figure 9.** Plots of the evolution of  $\bar{N}$  at  $\bar{y} = 0$  in time for four different current densities, using the expressions in equations (39) and (43). Also plotted are results from the numerical simulation (crosses), showing that the analytical expressions are very accurate. We see that the larger the current density, the shorter the amount of time the system will take to erode the current density within the original shear width.

The solution to this PDE falls into two distinct categories, depending on the value of  $\mathcal{W}$ , which is proportional to the current density, as indicated by equation (32).

#### 4.2.1. $\mathcal{W} < 1$ : No Broadening

[23] When

$$1 - \mathcal{W} = a^2 > 0 \quad (37)$$

then the solution to the PDE becomes

$$\bar{t} = \frac{1}{\bar{\alpha}} \int_1^{\bar{N}} \frac{d\bar{N}}{a^2 - \bar{N}^2} \quad (38)$$

since the ionosphere is initially undepleted (giving a lower limit of  $\bar{N} = 1$  in the integral). From this, we can obtain the profile of  $\bar{N}$  in time at  $\bar{y} = 0$ :

$$\bar{N}(\bar{y} = 0, \bar{t}) = a \left( \frac{1 + a + (1 - a) \exp(-2a\bar{\alpha}\bar{t})}{1 + a - (1 - a) \exp(-2a\bar{\alpha}\bar{t})} \right) \quad (39)$$

From this expression, we can see that  $\bar{N}(\bar{y} = 0, \bar{t} \rightarrow \infty) = a > 0$ , so in this regime, the ionospheric electrons are partially depleted within the original shear width, but the solution does not reach  $\bar{N} = 0$ , and no broadening of the depletion region occurs.

[24] We can see from this expression that the characteristic timescale for depletion in this regime is given by  $\bar{t}_d = (2a\bar{\alpha})^{-1}$ , giving a dimensional expression of

$$t_d = \frac{1}{2\alpha n_e \sqrt{1 - \mathcal{W}}} \quad (40)$$

#### 4.2.2. $\mathcal{W} > 1$ : Broadening

[25] When

$$1 - \mathcal{W} = -b^2 < 0 \quad (41)$$

then the solution to the PDE on  $\bar{y} = 0$  is given by

$$\bar{t} = -\frac{1}{\bar{\alpha}} \int_1^{\bar{N}} \frac{d\bar{N}}{b^2 + \bar{N}^2} \quad (42)$$

yielding

$$\bar{N}(\bar{y} = 0, \bar{t}) = b \tan \left( \arctan \left( \frac{1}{b} \right) - b\bar{\alpha}\bar{t} \right) \quad (43)$$

Thus, in this regime, depletion occurs all the way down to  $\bar{N} = 0$ , and this occurs at

$$\bar{t}_0 = \frac{1}{\bar{\alpha}b} \arctan \left( \frac{1}{b} \right) = \frac{\arctan(1/\sqrt{\mathcal{W}-1})}{\bar{\alpha}\sqrt{\mathcal{W}-1}} \quad (44)$$

We can use the expressions in equations (39) and (43) to plot  $\bar{N}(\bar{y} = 0, t)$ , as shown in Figure 9 for the same cases as those illustrated in Figure 3. Figure 9 shows that the larger the current density required, the quicker it erodes the number density at  $\bar{y} = 0$ : this makes sense, as a higher current density will remove more electrons  $\text{m}^{-2} \text{s}^{-1}$ .

[26] Since larger current densities take a relatively small time to dig down to  $\bar{N} = 0$ , we can find an estimate of the depletion time from the exponential in equation (31). This gives  $\bar{t}_d = \bar{\alpha}^{-1}$ , yielding a dimensional expression of

$$t_d = \frac{1}{\alpha n_e} \quad (45)$$

This depletion time is seen to be independent of initial current density. Figure 10 shows how this estimate of the depletion time varies with E region number density. It tells us that the depletion time is shorter ( $\sim 10$  s) for higher dayside number densities and rises to  $\sim 100$  s as the number density falls on the nightside. These estimates agree well with similar broadening observed by *Aikio et al.* [2004] over 70 s, and by *Marklund et al.* [2001] over 280 s.

[27] It may seem counterintuitive that the depletion time decreases as number density increases, since surely more electrons would take a longer time to deplete. Consider doubling  $n_e$  while keeping  $\alpha$  and  $\mathcal{W}$  constant. Equation (32) then tells us that  $j_{\parallel 0}$  will quadruple. Then, integrating equation (8) in the  $y$  direction gives us the total current,  $I$ , which remains constant in time: using equation (18) tells us that  $I = j_{\parallel 0} y_0$ . Thus the total current quadruples as well. So, while the number density has doubled, four times as many electrons are being drawn out per second, resulting in a halved depletion time. Another way of seeing this is to note that if  $n_e$  is doubled, the strength of the source term in equation (1) quadruples. The corresponding new solution (with  $\mathcal{W}$  unchanged) must have all the sources and sinks

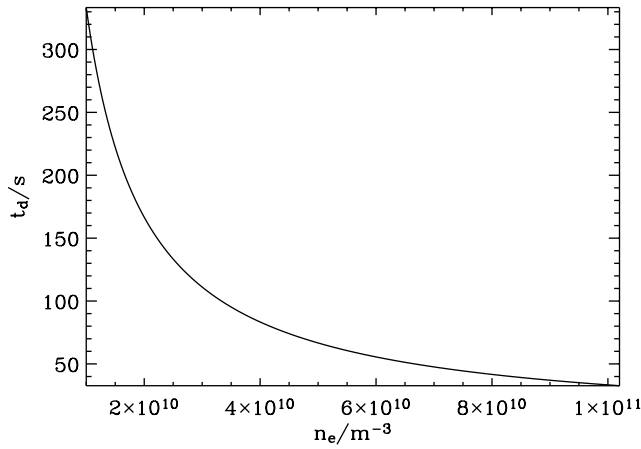


**Figure 10.** Plot of the characteristic depletion time,  $t_d$ , given in equation (45) in the broadening regime where  $j_{\parallel 0} > j_c$  or  $\mathcal{W} > 1$ . It shows that the lower the E region number density, the longer it takes for the system to reach equilibrium. Thus, for typical nightside number densities,  $t_d \sim 100$  s, but on the dayside with higher number densities,  $t_d \sim 10$  s.

increase in similar fashion, so the net extraction rate of electrons will quadruple also, while the number of electrons has only doubled.

[28] Figure 11 shows simulation depletion times calculated using the method described above, as well as the estimate above multiplied by  $\ln 2$  to account for the fact that the simulation depletion time is taken to be when half the total number of electrons have been depleted. The estimate is seen to provide a good indication of the characteristic depletion time, although immediately above  $j_c$ , we underestimate the depletion time slightly, as we have not allowed for the initial erosion in the region  $y < y_0$ . However, as the current density increases, the numerical results are seen to asymptote to the analytical approximation. The depletion is seen to take place over a characteristic timescale of  $\sim 20$ – $60$  s, again in good agreement with data.

[29] We can write our depletion time estimate as

$$t_d = \begin{cases} 1/\alpha n_e & : j_{\parallel 0} > j_c \\ 1/2\alpha n_e \sqrt{1 - \mathcal{W}} & : j_{\parallel 0} \leq j_c \end{cases} \quad (46)$$

## 5. Comparison With Data

[30] We now compare our simulation with the data from *Marklund et al.* [2001] (Figure 3b). Figure 3b shows that the region of downward current expands from 15 km [*Marklund et al.*, 2001] to 51 km at ionospheric level in 280 s, assuming that the first and last spacecrafts travel at the same speed through the structure. Thus, since our model is symmetric about the  $y$  axis, we take  $y_0 = 7.5 \times 10^3$  m, and we want to model broadening of  $\mathcal{W} = 51/15 = 3.4$ . The initial current density at Cluster's altitude of 21,000 km ( $r = 4.3 R_E$ ) is  $0.16 \mu\text{A m}^{-2}$ ; we need to know how this maps to iono-

spheric level, where  $r = R_E$ . The flux tube area scale factor is given by

$$F_A = \frac{r^3}{\sqrt{1 + 3 \sin^2 \theta}} \quad (47)$$

where  $r$  and  $\theta$  are polar coordinates, and on a flux tube

$$\frac{r}{R_E} = L \cos^2 \theta \quad (48)$$

where  $L$  is L shell. The event occurred at a magnetic latitude of  $69.8^\circ$ , which corresponds to the invariant latitude,  $\theta_I$ , at ionospheric level where  $r = R_E$ . Substituting these values into equation (48), we find that  $L = 8.39$ . From this, we can work out that the polar angle at the Cluster altitude of  $r = 4.3 R_E$  is  $\theta_c = 44.3^\circ$ . Using these values, we can find the ratio of  $F_A$  in equation (47) at ionospheric level and Cluster altitude to be

$$\frac{F_A^{\text{iono}}}{F_A^{\text{cluster}}} = 96.7 \quad (49)$$

which tells us that the initial current density for this event at ionospheric level is given by  $j_{\parallel 0} = 15.5 \mu\text{A m}^{-2}$ . This shows that we are examining a strong downward current event, where ionospheric electron depletion and broadening should both be important factors. Since we do not know from the data what the ionospheric number density is, we use equation (32) with  $\alpha = 3 \times 10^{-13} \text{ m}^3 \text{ s}^{-1}$  and  $h = 20$  km to infer that  $n_e = 6.88 \times 10^{10} \text{ m}^{-3}$ . This event occurred at 0336 MLT, so this number density is relatively large but reasonable for the nightside E region.

[31] With these parameter values, we can calculate the normalized quantities necessary for the numerical simula-

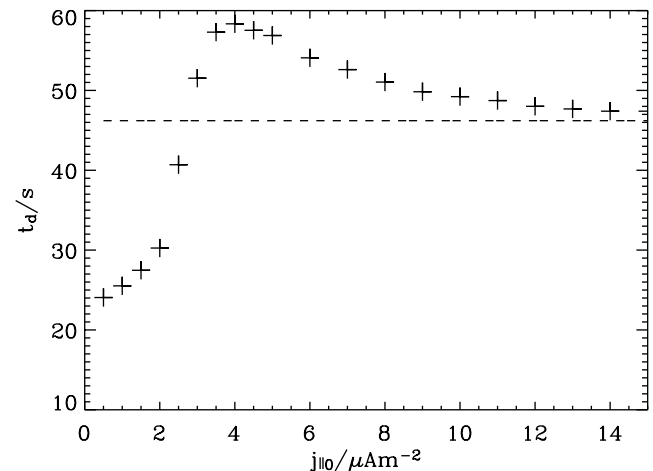


**Figure 11.** Simulation depletion times (crosses) and estimate (dashed line for  $j_{\parallel 0} > j_c$  estimate) from equation (46) for varying initial current densities. The estimate is multiplied by  $\ln 2$  to account for the fact that the crosses represent the time to half depletion: We see that the simulation depletion times asymptote toward the estimate as the current density increases.

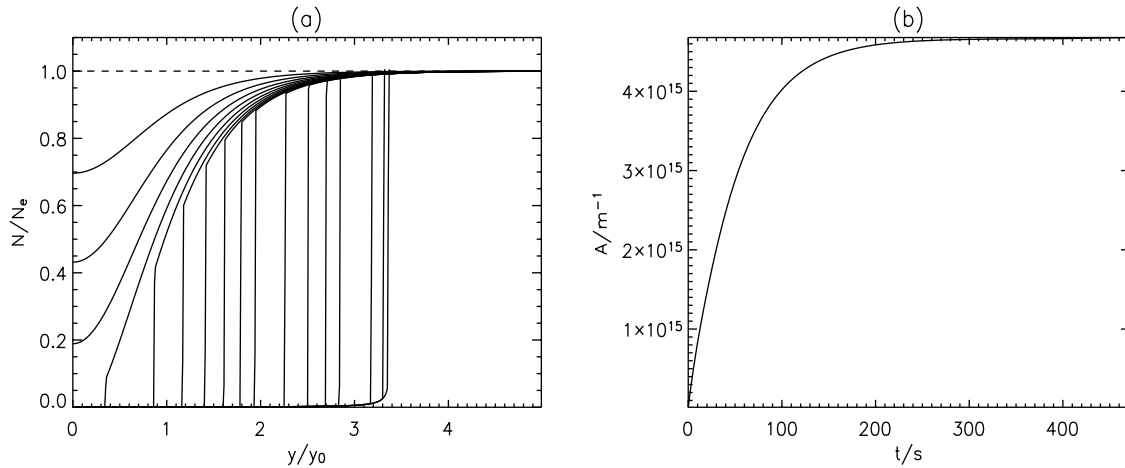


**Figure 12.** Comparison with *Marklund et al.*'s [2001] Figure 3. (a) Snapshots of number density profile show depletion to  $y = 3.4y_0$ , corresponding to 51 km. Number density profiles are shown for  $t = 0.0, 4.7, 9.4, 14.1, 18.9, 23.6, 28.3, 33.0, 37.7, 42.4, 47.1, 58.9, 70.7, 82.5, 94.3, 141.4, 188.6,$  and  $235.7$  s. (b) Number of depleted electrons,  $A$ , showing that the time for total depletion to occur is  $\sim 200$ – $300$  s, agreeing well with the satellite data.

tion using equations (9), (10), and (16):  $\beta = 1370$ ,  $\eta = 0.454$  and  $\bar{\alpha} = 9.73 \times 10^{-5}$ . Equation (18) tells us that the shear flow is  $u_{i0} = 1.59 \times 10^6 \text{ m s}^{-1}$ , yielding  $\tau = 4.71 \times 10^{-3}$  (equation (15)). Running our simulation with these parameters gave results shown in Figure 12: Figure 12a shows the number density contours, giving depletion to  $y = 3.4 y_0$  (51 km), while Figure 12b shows the number of depleted electrons,  $A(t)$ , defined in equation (35). This asymptotes to a constant value as the steady state is reached, and Figure 12 shows that full broadening has occurred after  $\sim 200$ – $300$  s, similar to the timescale of broadening seen in the Cluster data  $\sim 100$  s. This good comparison with data lends confidence to the results of our model and simulations.

## 6. Discussion and Conclusions

[32] We have used an Alfvén wave model of magnetosphere-ionosphere interaction to describe the ionospheric E region number density evolution under the influence of downward field-aligned current, photoionization and recombination. The flow of a downward field-aligned current, set up via a shear flow in the magnetosphere, leads to the evacuation of electrons from the E region up into the magnetosphere. The system reaches a steady state when the electron loss and production rates balance.

[33] This model assumes that the Alfvén wave which is launched in the magnetosphere is reflected back indefinitely; this assumption can be problematic on two levels. First, gradients in the Alfvén speed in the topside ionosphere can lead to partial Alfvén wave reflection on timescales of seconds [Lysak, 1990, 1991, and references therein]. *Streltsov and Lotko* [2003] have shown that the downward current region plays a major role in the formation of this feedback instability, since depleted plasma density and conductivity lower the threshold for instability onset. Secondly, even if the Alfvén wave progresses beyond the topside ionosphere without reflection, it will eventually reach the flow generator region, where interactions will take place [e.g., *Vogt et al.*, 1999]. Since a typical Alfvén

bounce time is of the order of ten to a hundred seconds, which is comparable to the depletion timescales considered in this paper, this interaction would become important.

[34] Nevertheless, our model is valuable in that it gives much insight into the interaction of downward current Alfvén waves with the ionosphere. Moreover, the assumption of an unimpeded reflected wave may be quite reasonable for lobe field lines or those in the plasma sheet boundary layer (PSBL), which are effectively open for the timescales of interest. Indeed, the data reported by *Marklund et al.* [2001], which our model describes well, were recorded in the PSBL.

[35] In our model, the behavior of the E region falls into two regimes: If the current density is small enough ( $j_{\parallel 0} < \alpha \epsilon n_e^2 h$  or  $\mathcal{W} < 1$ ), then the E region is partially depleted within the original shear flow width ( $y < y_0$ ), and reaches steady state before total depletion has occurred; when the current density is larger ( $j_{\parallel 0} > \alpha \epsilon n_e^2 h$  or  $\mathcal{W} > 1$ ), the E region becomes totally depleted within the original shear width and the current region is forced to broaden. On the dayside, where E region number densities are typically  $\sim 10^{11} \text{ m}^{-3}$  or more, broadening only occurs for strong current densities above  $10 \mu\text{A m}^{-2}$ , whereas on the nightside, where E region number densities can fall by a factor of 10 due to reduced production processes, broadening occurs for any downward current greater than  $\sim 0.1 \mu\text{A m}^{-2}$ . Thus our model predicts that significant E region depletion and current region broadening should be much more common on the nightside than on the dayside. The observations of current region broadening and depleted ionospheric number densities by *Marklund et al.* [2001] and *Aikio et al.* [2004] were all in the postmidnight sector, offering some support for our conclusions.

[36] We have derived expressions estimating the depletion width (generally  $\sim 1$ – $10 y_0$ ) and characteristic timescale of depletion ( $\sim 10$ – $100$  s). The timescales agree well with simulations by *Karlsson and Marklund* [1998], who find that depletions are noticeable on the order of seconds.

We have directly compared our model with Cluster data from *Marklund et al.* [2001] and were able to estimate the depletion time with accuracy, given the observed broadening width and other parameters.

[37] The results of this model compare favorably with those of *Streltsov and Marklund* [2006]: When they numerically modeled the Cluster data from *Marklund et al.* [2001], they were able to reproduce similar current density and dipolar diverging electric field profiles. Their results show that the magnitude of the current density decreases with time in the center of the current channel, in the same way as it does in our model. They also found that larger current densities and lower equilibrium E region number densities both lead to a broader current channel, in agreement with our findings.

[38] The source of electrons for the upward current is the magnetosphere, which can give an almost limitless supply [*Wright et al.*, 2002]. In contrast, the electrons which carry the downward current are supplied by the E region, a finite resource. This paper has demonstrated how important the magnetosphere-ionosphere boundary is to the evolution of the downward field-aligned current, and how the E region cannot simply be regarded as a limitless source of current carriers, since total depletion can occur in  $\sim 30$  s. A modification to this model could be the inclusion of the dense, thick (150–500 km altitude) F region which could also form part of the current circuit: This would have the effect of reflecting some of the incoming Alfvén wave at the magnetosphere-F region boundary, so that the Alfvén wave which reaches the E region has already been modified. This extra feature would give a better picture of the evolution of a downward current region and the associated accelerating potentials.

[39] **Acknowledgments.** Alexandra Cran-McGreehin is a PPARC Postdoctoral Fellow, and this work was started while she was supported by a Carnegie Trust Postgraduate Studentship. Amitava Bhattacharjee thanks the reviewers for their assistance in evaluating this paper.

[40] Amitava Bhattacharjee thanks the reviewers for their assistance in evaluating this article.

## References

- Aikio, A. T., T. Lakkala, A. Kozlovsky, and P. J. S. Williams (2002), Electric fields and currents of stable drifting auroral arcs in the evening sector, *J. Geophys. Res.*, *107*(A12), 1424, doi:10.1029/2001JA009172.
- Aikio, A., T. K. Mursula, S. Buchert, F. Forme, O. Amm, G. Marklund, M. Dunlop, D. Fontaine, A. Vaivads, and A. Fazakerley (2004), Temporal evolution of two auroral arcs as measured by the Cluster satellite and coordinated ground-based instruments, *Ann. Geophys.*, *22*, 4089.
- Blixt, E. M., and A. Brekke (1996), A model of currents and electric fields in a discrete auroral arc, *Geophys. Res. Lett.*, *23*, 2553.
- Cran-McGreehin, A. P., and A. N. Wright (2005a), Electron acceleration in downward auroral field-aligned currents, *J. Geophys. Res.*, *110*, A10S15, doi:10.1029/2004JA010898.
- Cran-McGreehin, A. P., and A. N. Wright (2005b), Current-voltage relationship in downward field-aligned current region, *J. Geophys. Res.*, *110*, A10S10, doi:10.1029/2004JA010870.
- Doe, R. A., J. F. Vickrey, and M. Mendillo (1995), Electrodynamical model for the formation of auroral ionospheric cavities, *J. Geophys. Res.*, *100*(A6), 9683.
- Jasperse, J. (1998), Ion heating, electron acceleration, and the self-consistent parallel electric field in downward current regions, *Geophys. Res. Lett.*, *25*, 3485.
- Karlsson, T., and G. Marklund (1998), Simulations of effects of small-scale auroral current closure in the return current region, *Phys. Space Plasmas*, *15*, 401.
- Knight, S. (1973), Parallel electric fields, *Planet. Space Sci.*, *21*, 741.
- Lysak, R. L. (1990), Electrodynamical coupling of the magnetosphere and ionosphere, *Space Sci. Rev.*, *52*, 33.
- Lysak, R. L. (1991), Feedback instability of the ionospheric resonant cavity, *J. Geophys. Res.*, *96*, 1553.
- Lysak, R. L., and Y. Song (2002), The role of Alfvén waves in the formation of auroral parallel electric fields, in *Magnetospheric Current Systems*, *Geophys. Monogr. Ser.*, vol. 118, edited by S. Ohtani et al., p. 173, AGU, Washington, D. C.
- Malinckrodt, A. J., and C. W. Carlson (1978), Relations between transverse electric fields and field-aligned currents, *J. Geophys. Res.*, *83*, 1426.
- Marklund, G. T., et al. (2001), Temporal evolution of the electric field accelerating electrons way from the auroral ionosphere, *Nature*, *414*, 724, doi:10.1038/414724a.
- Miura, A., and T. Sato (1980), Numerical simulation of global formation of auroral arcs, *J. Geophys. Res.*, *85*, 73.
- Pokhotelov, D., W. Lotko, and A. V. Streltsov (2002), Harmonic structure of field line eigenmodes generated by ionospheric feedback instability, *J. Geophys. Res.*, *107*(A11), 1363, doi:10.1029/2001JA000134.
- Sato, T. (1978), A theory of quiet auroral arcs, *J. Geophys. Res.*, *83*, 1042.
- St.-Maurice, J.-P., and P. J. Laneville (1998), Reaction rate of  $O^+$  with  $O_2$ ,  $N_2$  and  $NO$  under highly disturbed auroral conditions, *J. Geophys. Res.*, *103*(A8), 17519.
- Streltsov, A. V., and W. Lotko (2003), Small-scale electric fields in downward auroral current channels, *J. Geophys. Res.*, *108*(A7), 1289, doi:10.1029/2002JA009806.
- Streltsov, A. V., and W. Lotko (2005), Ultra-low-frequency electrodynamic of the magnetosphere-ionosphere interaction, *J. Geophys. Res.*, *110*, A08203, doi:10.1029/2004JA010764.
- Streltsov, A. V., and G. T. Marklund (2006), Divergent electric fields in downward current channels, *J. Geophys. Res.*, *111*, A07204, doi:10.1029/2005JA011196.
- Temerin, M., and C. W. Carlson (1998), Current-Voltage relationship in the downward current region, *Geophys. Res. Lett.*, *25*, 2365.
- Ulich, T., E. Turunen, and T. Nygrén (2000), Effective recombination coefficient in the lower ionosphere during bursts of auroral electrons, *Adv. Space Res.*, *25*(1), 47.
- Vedin, J., and K. Rönnmark (2004), A linear auroral current-voltage relation in fluid theory, *Ann. Geophys.*, *22*, 1719.
- Vickrey, J., R. Vondrack, and S. Matthews (1982), Energy deposition by precipitating particles and Joule dissipation in the auroral ionosphere, *J. Geophys. Res.*, *87*(A7), 5184.
- Vogt, J., G. Haerendel, and K. H. Glassmeier (1999), A model for the reflection of Alfvén waves at the source region of the Birkeland current system: The tau generator, *J. Geophys. Res.*, *104*(A1), 269.
- Wright, A. N. (1996), Transfer of magnetosheath momentum and energy to the ionosphere along open field lines, *J. Geophys. Res.*, *101*(A6), 13,169.
- Wright, A. N., and A. W. Hood (2003), Field-aligned electron acceleration in Alfvén waves, *J. Geophys. Res.*, *107*(A3), 1135, doi:10.1029/2002JA009551.
- Wright, A. N., W. Allan, M. S. Ruderman, and R. C. Elphic (2002), The dynamics of current carriers in standing Alfvén waves: Parallel electric fields in the auroral acceleration region, *J. Geophys. Res.*, *107*(A7), 1120, doi:10.1029/2001JA900168.

A. P. Cran-McGreehin, A. W. Hood, and A. N. Wright, Department of Mathematical and Computational Sciences, Mathematical Institute, Room M212, University of St. Andrews, North Haugh, St. Andrews, Fife KY16 9SS, UK. (alex@mcs.st-and.ac.uk; andy@mcs.st-and.ac.uk; alan@mcs.st-and.ac.uk)